HTML ABSTRACT + LINKS

JOURNAL OF APPLIED PHYSICS VOLUME 95, NUMBER 5 1 MARCH 2004

APPLIED PHYSICS REVIEWS—FOCUSED REVIEW

High-efficiency AlGaInP light-emitting diodes for solid-state lighting applications

Th. Gessmann[a)] and E. F. Schubert
Department of Electrical, Computer, and Systems Engineering, Rensselaer Polytechnic Institute, Troy, New York 12180

(Received 11 July 2003; accepted 1 December 2003)

AlGaInP lattice matched to GaAs is suited for light-emitting diodes (LEDs) operating in the red, orange, yellow, and yellow–green wavelength range. Such long-wavelength visible-spectrum devices will play an important role in solid-state lighting applications. This review discusses the major classes of AlGaInP device structures, including absorbing-substrate (AS) LEDs, absorbing substrate LEDs enhanced by distributed-Bragg-reflectors (DBRs), transparent substrate (TS) LEDs, thin-film (TF) LEDs, and LEDs using omnidirectional reflectors (ODRs). Some of these device structures have well-known deficiencies: A significant fraction of light is absorbed in the GaAs substrate in AS-LEDs; DBRs are essentially transparent at oblique angles of incidence leading to substantial optical losses. More recent developments such as TS-LEDs and TF-LEDs avoid these drawbacks. High-reflectivity, electrically conductive ODRs were recently developed that considerably outperform conventional distributed Bragg reflectors. LEDs using such conductive ODRs can replace DBRs in AlGaInP LEDs and are potential candidates for low-cost high-efficiency LEDs suitable for high-power solid-state lighting applications. *© 2004 American Institute of Physics.* [DOI: 10.1063/1.1643786]

TABLE OF CONTENTS

I. INTRODUCTION. 2203
II. AlGaInP LEDs IN SOLID-STATE LIGHTING APPLICATIONS. 2204
III. EARLY DEVELOPMENT OF THE AlGaInP MATERIAL SYSTEM. 2204
IV. ABSORBING-SUBSTRATE LEDs (AS LEDs)... 2205
V. DISTRIBUTED-BRAGG-REFLECTOR-ENHANCED ABSORBING SUBSTRATE LEDs (DBR-LEDs). 2205
VI. HIGH EXTRACTION STRATEGIES FOR AlGaInP LEDs. 2206
A. Transparent-substrate LEDs. 2206
B. Surface-textured LEDs. 2207
C. Photonic-crystal LEDs. 2208
D. Thin-film LEDs. 2208
VII. CONCEPTS FOR REFLECTING STRUCTURES. 2209
VIII. OMNIDIRECTIONAL REFLECTOR (ODR) FOR LEDs. 2210
IX. CHARACTERISTICS OF ODR-LEDs. 2211
X. WAFER BONDING FOR AlGaInP ODR-LEDs... 2214
XI. CONCLUSIONS. 2215

[a)]Author to whom correspondence should be addressed; electronic mail: gessmann@rpi.edu

I. INTRODUCTION

Early materials used for light-emitting diodes (LEDs) emitting in the long-wavelength part of the visible spectrum were GaP doped with isoelectronic impurities such as nitrogen and GaAsP (for a review, see Schubert).[1] These materials suffer from low efficiency and output power: GaAsP is lattice mismatched to GaAs and therefore has many dislocations; GaP:N lacks high-power capabilities due to the saturation of radiative recombination at high injection-current levels. AlGaAs is a high-efficiency material suitable for infrared and red wavelengths (for a review, see Steranka).[2] However it is unsuitable for orange and shorter wavelengths due to the direct-indirect transition of the $Al_xGa_{1-x}As$ band gap at $x \approx 45\%$ corresponding to a wavelength of 624 nm.

AlGaInP is the material of choice for the long-wavelength part of the visible spectrum, namely for red, orange, yellow, and yellow–green wavelengths. At the molar In composition of 50%, $(Al_xGa_{1-x})_{0.5}In_{0.5}P$ is lattice matched to GaAs. Unlike GaAsP, which is also grown on GaAs, AlGaInP does not suffer from lattice mismatch. Unlike GaP:N, AlGaInP does not rely on deep-level-mediated transitions that tend to saturate. Similar to AlGaAs, AlGaInP suffers from a direct-indirect transition of the band gap. However, the direct-indirect transition in AlGaInP occurs at a higher energy compared with AlGaAs. As a result, the AlGaInP materials system can be used for all colors of the long-wavelength region of the visible spectrum down to yellow–green wavelengths.

 © 2004 American Institute of Physics

Downloaded 10 Mar 2004 to 128.113.123.154. Redistribution subject to AIP license or copyright, see http://jap.aip.org/jap/copyright.jsp

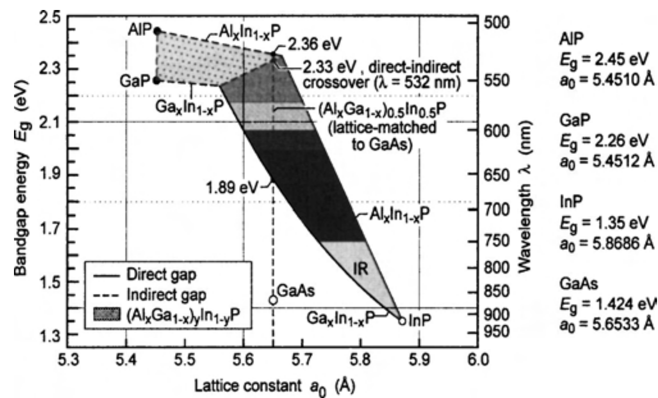

FIG. 1. Band gap energy and corresponding wavelength vs lattice constant of $(Al_xGa_{1-x})_yIn_{1-y}P$ at 300 K. The dashed vertical line shows $(Al_xGa_{1-x})_{0.5}In_{0.5}P$ lattice matched to GaAs (adopted from Ref. 4).

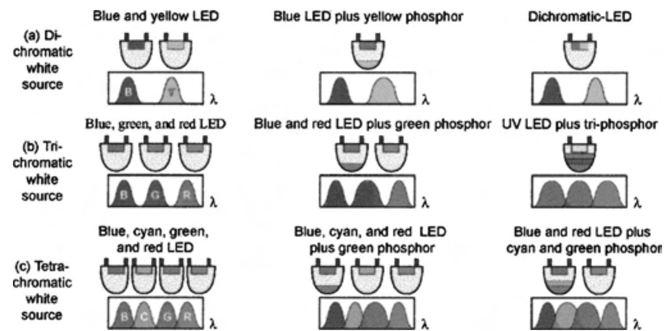

FIG. 2. LED-based approaches for white light sources and corresponding optical spectra. The highest luminous efficacy is provided by the dichromatic approaches. The best color rendering is obtained with tetrachromatic approaches. Trichromatic approaches based on LEDs can provide good color rendering as well as high luminous efficacy.

The AlGaInP band gap energy, the corresponding wavelengths, and the nature of the band gap (direct or indirect), are shown in Fig. 1. The vertical dashed line in the figure indicates the composition at which AlGaInP is lattice-matched to GaAs. The direct-indirect transition of the bandgap occurs at the energy of 2.23–2.33 eV corresponding to 556–532 nm. The exact energy at which the direct–indirect transition occurs depends on the degree of randomness of the quaternary alloy semiconductor and is lower for AlGaInP with a high degree of order.[3]

The importance of AlGaInP LEDs as an instrumental ingredient in future solid-state lighting systems will be reviewed. We will discuss the major technologies suitable for high-efficiency and high-power AlGaInP LEDs. Special emphasis will be placed on the discussion of the limitations of current AlGaInP technologies and on emerging technologies such as AlGaInP LED structures employing omnidirectional reflectors (ODRs) and thin-film (TF) technologies using pyramidal reflectors for enhanced light extraction.

II. AlGaInP LEDs IN SOLID-STATE LIGHTING APPLICATIONS

It is well known that semiconductor-based light sources have, in principle, the potential to achieving near-unity power efficiency. This is in contrast to common conventional light sources such as incandescent and fluorescent lamps that have fundamental efficiency limitations that prevent them from reaching near-unity efficiencies. As low-cost sources that provide high-efficiency and high power output are developed, semiconductor light sources will replace fluorescent and inefficient incandescent sources.

Different semiconductor-based schemes to generate white light for general daylight illumination applications are shown in Fig. 2. The figure shows different approaches for (a) dichromatic, (b) trichromatic, and (c) tetrachromatic white light sources including single-chip semiconductor sources and multichip semiconductor sources. The figure also shows semiconductor/phosphor-based sources including a blue LED/yellow phosphor source, a blue and red LED/green phosphor source, and an ultraviolet (UV) LED/phosphor source. Tetrachromatic approaches offer outstanding color rendering properties if the wavelength of each source and their temperature dependencies can be controlled accurately. As a result, there is little motivation to develop pentachromatic approaches, although such pentachromatic approaches may be suitable for certain niche markets.

Several characteristics of the solid-state white sources shown in Fig. 2 are noteworthy. First, dichromatic approaches have the highest luminous efficacy and they are well suited for display and indicator-light applications. Due to their low color rendering capabilities, their usefulness in daylight illumination and display backlighting applications is limited. Second, trichromatic approaches based on either LEDs or phosphors provide excellent color rendition with a Commission Internationale de l' Éclarge (CIE) general color-rendering index of 90 or higher.[5] Third, due to the unavoidable Stokes shift in the trichromatic UV-LED/phosphor source, the potential luminous efficiency of this source is lower compared with a trichromatic multichip LED approach. Fourth, the trichromatic approach shown in Fig. 2 consisting of a blue LED, a green phosphor, and a red LED is motivated by the unavailability of highly efficient green semiconductor-based emitters. The use of the red LED is motivated by the availability of efficient red AlGaInP LEDs. In addition, the employment of red LEDs allows for the avoidance of the very large Stokes shift concomitant with the UV or blue LED/red phosphor combination. Therefore, the two LED/green phosphor approach promises both, good efficiency and color rendering capabilities.

A detailed analysis[5] and the preceding discussion of different solid-state-lighting strategies make clear that the emission sources with the highest luminous efficiencies and excellent color rendering properties ($\geqslant$90) include red LEDs. With luminous efficiency and the resulting energy savings as strong driving forces for solid-state lighting, large-scale use of AlGaInP LEDs is expected in future lighting systems.

III. EARLY DEVELOPMENT OF THE AlGaInP MATERIAL SYSTEM

The AlGaInP material system was developed in Japan for visible lasers.[6–9] Efforts started with AlGaInP/GaInP double-heterostructure lasers using $Ga_{0.5}In_{0.5}P$ as the light-emitting active material, which is lattice matched to GaAs

Downloaded 10 Mar 2004 to 128.113.123.154. Redistribution subject to AIP license or copyright, see http://jap.aip.org/jap/copyright.jsp

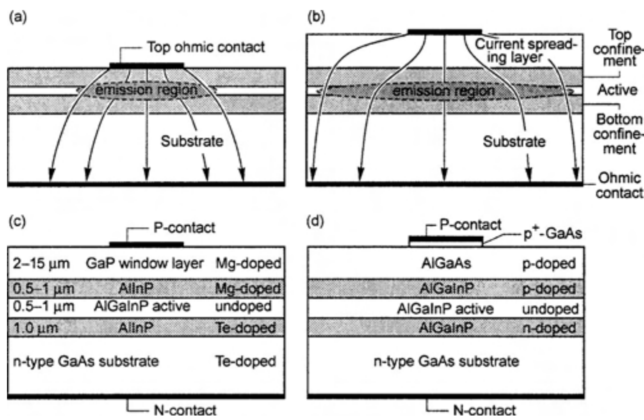

FIG. 3. Current distribution and light-generating region in an AlGaInP LED: (a) without and (b) with a spreading layer. (c) GaP current-spreading structure (see Refs. 14 and 18). (d) AlGaAs current-spreading structure (see Refs. 19 and 20).

substrates. The bandgap energy of lattice-matched (random alloy) GaInP is approximately 1.9 eV (650 nm), making the material suitable for visible lasers emitting in the red. These lasers are used, for example, in digital versatile disc technology and in laser pointers. The addition of Al to GaInP allows one to attain shorter emission wavelengths including the orange and yellow spectral region. However, $(Al_xGa_{1-x})_{0.5}In_{0.5}P$ becomes an indirect semiconductor at Al compositions of $x \approx 0.53$, so that the radiative efficiency strongly decreases at wavelengths near and, in particular, below 600 nm. Consequently, AlGaInP is not suited for high-efficiency emission at wavelengths below 570 nm. Reviews of different aspects of the AlGaInP material system and AlGaInP LEDs can be found in the literature.[1,10–12]

IV. ABSORBING-SUBSTRATE LEDs (AS LEDs)

Subsequent to the AlGaInP laser development that occurred in the early 1980s, AlGaInP LED development started at the end of the 1980s and early 1990s.[13–16] These LEDs were grown in a *p*-side-up configuration on conductive *n*-type GaAs substrates.

In contrast to the AlGaInP laser structures, LED structures employ current-spreading layers. The effect of the current-spreading or window layer is shown in Fig. 3. Without a current-spreading layer the current is maximal under the center of the top contact, as shown in Fig. 3(a). Because most of the light is generated in the region below the opaque top contact, the light extraction efficiency of AlGaInP LEDs without a current-spreading layer is low. The effect of the current spreading layer is shown in Fig. 3(b). For a sufficiently thick and conductive current-spreading layer, the entire $p-n$ junction plane of the LED chip lights up and not just the region below the top ohmic contact. It is desirable to spread the current beyond the contact area by a distance larger than the contact radius. However, spreading the current all the way to the edge of the chip could result in unwanted surface recombination.

The theory of current spreading has been well understood for *stripe-like* contacts as used in lasers.[17] Recently, the current spreading length was derived for a *circular* contact geometry, commonly used in LEDs.[1] For such circular contacts, the thickness t of the current-spreading layer required to attain a current-spreading length of L_s is given by

$$t = \rho L_s \left(r_c + \frac{L_s}{2} \right) \ln\left(1 + \frac{L_s}{r_c} \right) \left(\frac{J_0 q}{n_{\mathrm{ideal}} kT} \right), \tag{1}$$

where ρ is the resistivity of the current spreading layer, r_c is the contact radius, J_0 is the current density at the edge of the contact, n_{ideal} the diode-ideality factor, q the elementary charge, k the Boltzmann constant, and T is the absolute temperature.

Equation (1) is different from the commonly used formula for stripe-shaped contacts, where the required thickness is given by (Thompson[17])

$$t = \rho L_s^2 \frac{J_0 q}{n_{\mathrm{ideal}} kT}. \tag{2}$$

Using the approximation $\ln(1+x) \approx x$, valid for small values of x, allows one to show that Eqs. (1) and (2) yield the same result in the limit of $r_c \to \infty$.

Two types of current-spreading layers have been employed in AlGaInP LEDs, namely AlGaAs[15,16] and GaP.[13] AlGaAs is lattice matched to GaAs and, at sufficiently high Al mole fractions, is transparent to red light. The band gap of AlAs is 2.17 eV corresponding to 571 nm. If high percentages of Al are employed, AlGaAs tends to oxidize and its semiconducting properties deteriorate. An alternative current-spreading material in GaP, which has a band gap energy of 2.26 eV corresponding to 548 nm. GaP is lattice mismatched to GaAs but long-term stable and more transparent than AlGaAs. The deleterious consequences of the lattice mismatch between the AlGaInP upper cladding layer and the GaP window layer can be minimized by placing the mismatched interface sufficiently far away from the active region to reduce carrier recombination at the mismatched interface.

Further improvements were attained by using multiple quantum well (MQW) active regions,[21] coherently strained MQW active regions,[22,23] distributed Bragg reflectors,[21,24,25] and transparent GaP substrate technology.[3] A major drawback of the AlGaInP LED shown in Fig. 3 is the absorbing nature of GaAs in the wavelength range of interest. The band gap of GaAs occurs at 870 nm so that all visible-spectrum photons are absorbed in GaAs substrates. Light emitted downward from the active region in AS-LEDs is absorbed by the GaAs substrate. The optical losses in AlGaInP LEDs incurred due to absorption effects in GaAs substrates are greater than 50%. Due to these losses, AlGaInP AS-LEDs have low efficiencies and output powers making them suitable for only low-power applications, e.g., indicator-light applications, and excluding them from solid-state lighting applications.

V. DISTRIBUTED-BRAGG-REFLECTOR-ENHANCED ABSORBING-SUBSTRATE LEDs (DBR-LEDs)

In order to improve the extraction efficiency of AlGaInP AS-LEDs, a distributed Bragg reflector (DBR) is included between the substrate and the lower cladding layer. The sche-

Downloaded 10 Mar 2004 to 128.113.123.154. Redistribution subject to AIP license or copyright, see http://jap.aip.org/jap/copyright.jsp

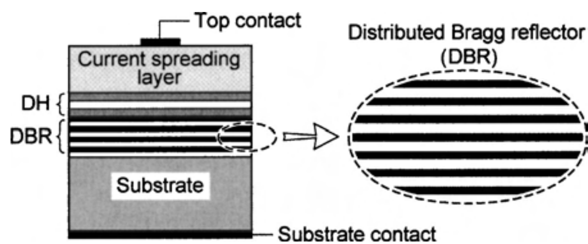

FIG. 4. AlGaInP LED with a distributed Bragg reflector (DBR) located between the substrate and the lower cladding layer.

matic structure of a DBR-enhanced AS LEDs (here referred to as DBR-LED) is shown in Fig. 4. Kato *et al.*[24] pioneered DBR-LEDs.

To evaluate the potential enhancement provided by the DBR, it is instructive to determine the DBR reflectivity as a function of wavelength and angle of incidence. The result of this evaluation is shown in Fig. 5 for DBRs designed for an emission wavelength of 630 nm. Two DBRs are shown in the figure, namely a transparent AlGaInP/AlInP and an absorbing AlGaAs/AlGaAs DBR. The transparent DBR has the advantage of low optical losses. However transparency can be attained only by high Al contents in the low-index as well as high-index layers, which in turn reduces the refractive index contrast. As a consequence, a large number of quarter wave pairs are needed for high reflectivity. On the other hand, the absorbing DBR allows for a higher index contrast. This enables the reduction of the number of quarter wave pairs to attain a certain reflectivity. Thus there is a tradeoff between number of pairs and maximum attainable reflectance in a DBR. Frequently a combination of absorbing and transparent layers in DBRs is used to maximize the reflectivity and minimize the number of quarter wave pairs.

Inspection of Fig. 5(a) reveals a high-reflectivity band with a width of more than 50 nm for the transparent DBR; this is wider than the emission linewidth of a typical AlGaInP LED. Figure 5(b) shows the reflectivity of the DBRs as a function of the angle of incidence. Inspection of the figure reveals a problematic issue, namely the low reflectivity of the DBR for oblique angles of incidence: For angles $20° < \phi < 70°$, the DBRs are essentially transparent. Thus light emitted by the active region in this range of angles can be transmitted by the DBRs and absorbed in the GaAs substrate.

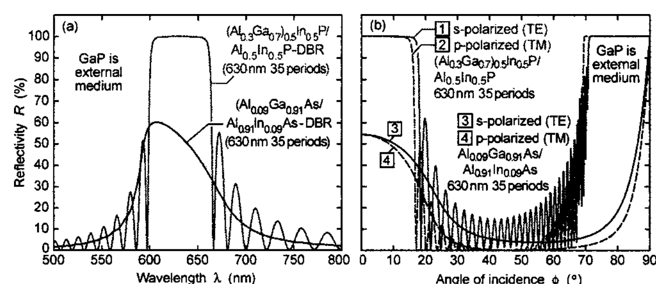

FIG. 5. (a) Reflectivity vs wavelength and (b) reflectivity vs angle of incidence for a transparent AlGaInP/AlInP DBR and an absorbing AlGaAs/AlGaAs DBR.

The optical power emitted by the active region into the solid-angle element given by ϕ and $\phi + d\phi$, where ϕ is assumed to be 0° at normal incidence, is given by the proportionality

$$P \propto r^2 \sin\phi \, d\phi. \tag{3}$$

The sinusoidal dependence indicates that angles near 0°, where the DBR has high reflectivity, have little importance. Angles $\gg 0°$ have greater importance due to the dependence of the sinus function on angle. However, the DBR has a low reflectivity in this range of angles, as displayed in Fig. 5. Thus the DBR's reflectivity characteristics leave substantial room for improvement. This point will be further discussed in a subsequent section on ODRs.

Figure 5 also shows that the DBR reflectivity increases again for grazing-angle incidence, namely for $\phi > 70°$. As a consequence, grazing-angle waveguided modes propagating in the top layers of the LED, namely the confinement, active, and window layers, will be supported by the DBR and guided to the edge of the die where they can escape.

VI. HIGH EXTRACTION STRATEGIES FOR AlGaInP LEDs

So far the AlGaInP material system has achieved one of the highest internal quantum efficiencies (close to 100% in the red wavelength range) of all semiconductors used for emission of visible light. It is therefore particularly important to develop LED structures with extraction efficiencies significantly exceeding the AS-LED and DBR-LED technologies. General aspects of AlGaInP LED technology have been the subjects of several reviews.[1,3,4,11] Here we briefly review commercially available high extraction efficiency structures in order to compare them later to the ODR-LEDs.

Early AlGaInP-based LEDs with external efficiencies η significantly exceeding GaAsP- and GaP-based devices ($\eta = 0.1\% - 0.6\%$) were obtained by using organometallic vapor phase epitaxy (OMVPE). The devices consisted of a double heterostructure with conductive AlGaAs window layers[15,16] or conductive GaP-window layers grown lattice mismatched with respect to the active region.[13] These LEDs attained external quantum efficiencies of about 3% or less in the wavelength range 555–620 nm ($I_f = 20$ mA dc).

Subsequently, a twofold increase in quantum efficiency was achieved by employing a very thick (45 μm) conductive GaP window layer grown by hydride vapor phase epitaxy on top of the OMVPE heterostructure.[26] The thick window layer allows maximizing the side extraction efficiency, which depends on the solid angle of intersection between the window layer sidewalls and the cone of acceptance for sideways directed light.[26] In addition, the thick window layer helps to spread the current beneath the top contact. Peak external efficiencies larger than 6% ($I_f = 20$ mA dc) have been reported for wavelengths > 600 nm.[26]

A. Transparent-substrate LEDs

The devices discussed so far employ the original GaAs substrate, which absorbs light emitted "downwards" from the active region or totally reflected at the LED top surface. This loss effect can be decreased either by covering the

Downloaded 10 Mar 2004 to 128.113.123.154. Redistribution subject to AIP license or copyright, see http://jap.aip.org/jap/copyright.jsp

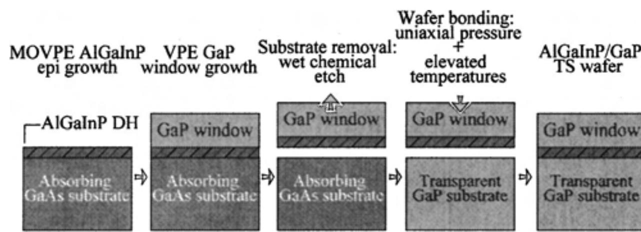

FIG. 6. Fabrication process of an AlGaInP TS LED. The LED structure is wafer bonded to a GaP substrate (adopted from Ref. 3).

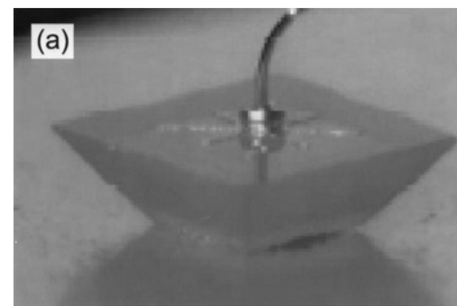

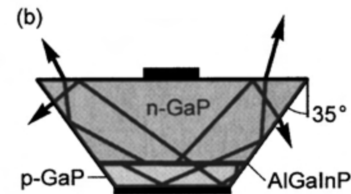

FIG. 7. TIP-LED structure (from Lumileds Corporation): (a) TIP LED under operation and (b) typical photon paths and escape possibilities (adopted from Ref. 33).

GaAs substrate with a DBR[20] or by replacing the GaAs substrate with a transparent substrate (TS).[27] Due to the small range of angles with high reflectance, the DBR results in a device which is primarily "top emitting," whereas a TS device allows for light emission from the edges of the chip and can therefore be much more efficient.

Similar to double-heterostructure AlGaAs LEDs with a transparent conductive AlGaAs substrate,[28] AlGaInP TS-LEDs utilize a transparent conductive GaP carrier. GaP is transparent for the entire range of AlGaInP emission wavelengths. The use of a conductive substrate supports current spreading above the patterned backside contacts of the LED.[27]

AlGaInP transparent substrate (TS) LEDs were pioneered by Kish *et al.*[27] who developed a technique to remove the original GaAs substrate and to join the LED epitaxial layer with a conductive GaP carrier by means of direct semiconductor-to-semiconductor waferbonding.[27,29,30] Figure 6 shows the schematic fabrication process, during which a semiconductor–wafer heterointerface is formed. However, the process requires crystallographic alignment, tight control of all process parameters, and suffers from the use of costly GaP substrates and increased forward voltages. Furthermore, the current lack of 4″ GaP substrates may delay the scalability of the TS process.

Kish *et al.*[27] reported external quantum efficiencies of 17.6% at 629 nm and luminous efficiencies of 41.5 lm/W at 604 nm ($I_f = 20$ mA dc). Further improvements have resulted in even higher values of the efficiencies: About 74 lm/W at 615 nm and more than 30% external quantum efficiency at 632 nm.[31]

In square-shaped TS-LEDs, several mechanisms limit the external quantum efficiency such as photon reabsorption in the active layer and free-carrier absorption in the doped GaP substrates. In devices with *thin* active layers (a few nanometers thick, as generally used in the AlGaAs–InGaAs–GaAs system) reabsorption processes may in fact *increase* the external quantum efficiency via photon-recycling effects.[32] However, due to the low barrier height, AlGaInP devices with peak wavelengths < 630 nm require relatively thick (several hundred nm) active layers to achieve sufficient electron confinement and are therefore subject to significant absorption losses in the active region. For such devices, the external efficiency can be increased by geometrically shaping the chips so as to minimize the path length of photons before extraction. Suitable chip structures for high extraction efficiencies may be spheres, hemispherical domes, or truncated ellipsoids. However, these structures are difficult to realize and therefore expensive.

Krames *et al.*[33] demonstrated a practical yet very efficient structure, the truncated-inverted pyramid (TIP) LED shown in Fig. 7. The sidewalls of the chip were beveled with a sidewall angle of 35° with respect to the vertical direction (see Fig. 7). The LED is mounted *n*-side up on a thermal heat sink in order to enhance heat removal from the device. The TIP structure redirects photons totally reflected at the sidewalls towards the top surface, where they arrive at a more advantageous angle and can be extracted. On the other side, photons totally reflected at the top surface can escape through the tilted sidewalls [see Fig. 7(b)].

The performance of AlGaInP TIP-LEDs exceeds 100 lm/W at 100 mA dc for emission at 610 nm. Record external quantum efficiencies of 55% under dc operation ($I_f = 100$ mA) were achieved at 650 nm.[33] At the same forward current under low duty cycle operation, the external quantum efficiency increased to 60.9%, which indicates a lower bound for the extraction efficiency of the TIP-LED.[33]

B. Surface-textured LEDs

Chip surfaces may be textured in order to increase the light extraction efficiency. An advantage of this approach is that it leads to a scalable chip design as opposed to the chip shaping techniques discussed above. A possibility of structuring consists of randomly roughening the upper window layer. This can be achieved, e.g., using polystyrene spheres and dry etching.[34] In this case, photons incident at the roughened surface are either scattered isoptropically (and can escape from the chip) or reflected with a random distribution of the reflection angles. As a result, the probability of light extraction is increased on multiple round trips between surface and substrate (assuming the substrate is covered by a high-reflectivity mirror). To maximize this effect, a highly reflective wide-angle mirror should be inserted between the substrate and lower confinement layer; this, however, requires

Downloaded 10 Mar 2004 to 128.113.123.154. Redistribution subject to AIP license or copyright, see http://jap.aip.org/jap/copyright.jsp

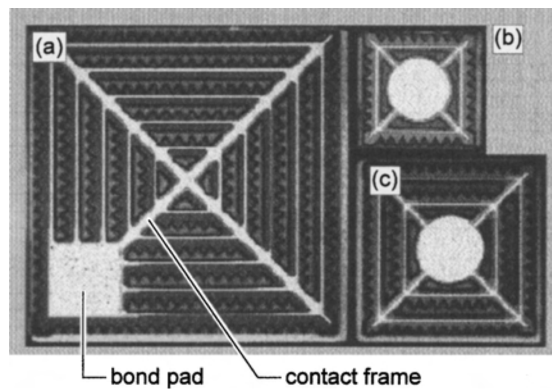

FIG. 8. Top view of surface-textured AlGaInP LEDs with different areas, geometrical patterns, and contact frames (adopted from Ref. 36). (a) High-current chip (drive current 400 mA, $500\times500\ \mu m^2$ die). (b) Low-current chip (drive current 30 mA, $200\times200\ \mu m^2$ die). (c) Standard chip (drive current 70 mA, $300\times300\ \mu m^2$ die).

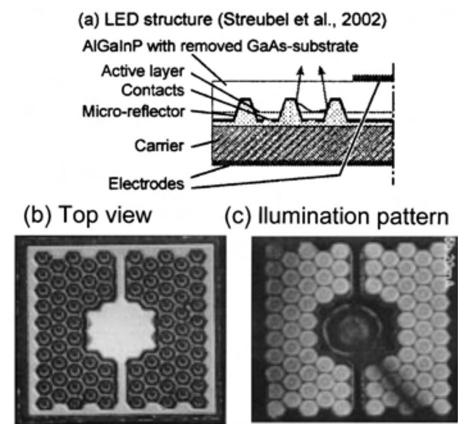

FIG. 9. (a) Schematic structure and photograph of (b) uninjected and (c) current-injected AlGaInP thin-film LED with pyramidal microreflectors. Current is injected through the bond pad and a square frame along the edged of the *n*-type top contact layer. Individual *p*-type contacts are discernable as dark spots in (b) due to the transparency of the upper window and active layer (adopted from Ref. 37).

removal of the original substrate and transfer of the LED to another carrier. In addition, the thickness of the active region needs to be optimized to reduce absorption losses. External efficiencies of 46% for GaAS-based LEDs with randomized surface structure have been reported.[35]

Another approach is based on *regular* patterns of geometrical structures on the top surface of the LED (see Fig. 8). This has been realized using truncated tetrahedrons or other shapes etched into the window layer of an AlGaInP AS-LED.[36,37] The two-dimensional pattern of tetrahedrons enhances the effective surface area available to light extraction and offers a variety of surfaces at different tilt angles. Photons entering a single tetrahedron can undergo multiple total reflection events at the sidewalls guiding them in such a way that the incidence angle progressively increases and eventually may fall within the escape cone. However, since current spreading is strongly obstructed in etched regions, a contact frame on top of the window layers is needed to ensure uniform current injection across the LED surface. In addition, a specially designed wide-angle Bragg reflector is used to recover a large part of the radiation emitted towards the substrate side of the LED. For packaged devices emitting at around 610 nm luminous performances larger than 30 lm/W and typical operating voltages below 2.2 V have been achieved.[36]

C. Photonic-crystal LEDs

Two-dimensional photonic crystals included in the upper window layer are examples for periodical structures with a characteristic length scale of the order of the emitted wavelength. The photonic crystal can be designed to Bragg scatter light, which is trapped in wave-guided modes, into light modes radiating through the top surface. This concept was used by Erchak *et al.*[38] who demonstrated a sixfold photoluminescence (PL) intensity increase utilizing a triangular lattice etched into the upper window layer of an InGaP/InGaAs LED emitting at 935 nm.

However, nonradiative carrier recombination and surface recombination are increased near the etched interfaces. This can pose a problem when the lattice constant of the photonic crystal becomes comparable to the carrier diffusion length in the active region. It is therefore important to avoid penetrating the active region with the photonic crystal. While photonic crystals in general result in far-field patterns different from flat-surface rectangular-parallelepiped-shaped LEDs, other surface structuring techniques maintain the Lambertian emission pattern.[37]

D. Thin-film LEDs

An alternative to TS-LEDs, offering high-extraction efficiency, is made possible by TF technology. Here the epitaxial layer is removed from the original GaAs substrate and transferred to a another carrier by means of metal-to-metal bonding (see Figs. 9 and 10). Stringent semiconductor-to-semiconductor wafer bonding process parameters such as ultraflat surfaces and crystallographic orientation matching are not required for TF-LEDs.

Illek *et al.*[39] demonstrated a TF AlGaInP LED with an array of buried coneshaped microreflectors. The LED structure is shown schematically in Fig. 9. The cones are etched through the active layer and covered by a metal and a thin dielectric layer. Small openings in the dielectric provide for electrical conductivity and localize current injection and light generation to the center of the cones. The shape of the microreflectors is designed such that totally reflected light is

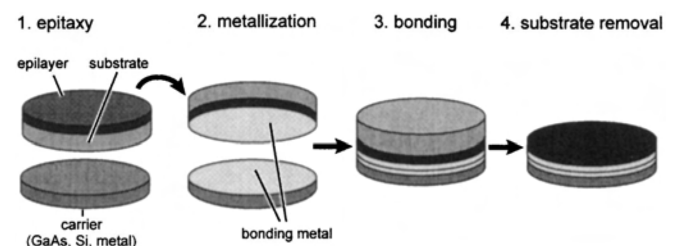

FIG. 10. Wafer bonding processing steps for thin film LED technology utilizing metal-to-metal bonding by means of soldering (adopted from Ref. 39).

Downloaded 10 Mar 2004 to 128.113.123.154. Redistribution subject to AIP license or copyright, see http://jap.aip.org/jap/copyright.jsp

guided upwards. As a result, the TF-LED with buried microreflectors is predominantly top emitting. In contrast to TS-LEDs, very thick window layers in order to increase sidelight extraction are not required.[37,39] For devices emitting at 650 nm, quantum efficiencies of 31%[40] and 40%[41] have been reported. Despite the presence of etched regions, the forward voltage is below 2.0 V at a forward current $I_f = 10$ mA.[37,39]

There are disadvantages to the TF-LED structure, namely the fact that the ratio of current-injected area to chip area is small. Analysis of the schematic of Fig. 9(a) and the photographs of Fig. 9(b) shows that this ratio is less than 10%. Furthermore, the microreflectors penetrate the active layer, thereby subjecting carriers to the possibility of nonradiative interface recombination.

The semiconductor–metal interface should be highly reflective and form a low-resistance ohmic contact to the conducting carrier. The last requirement can be dropped for TF-LEDs using insulating carriers.[42,43] For insulating carriers, two side-by-side top contacts are required. Other important requirements are matching of thermal expansion coefficients between the LED epilayer, bonding material and carrier, and good thermal conductivity of the carrier.

Figure 10 shows a schematic wafer bonding process where the LED epilayer covered by a metal such as Au and the carrier covered by a solder metal such as AuSn are brought in contact and heated. During this step, during which the wafers are kept at low temperatures (350 °C) to avoid dopant redistribution, a stable metal-to-metal bond is formed.[37,39] This bond is able to sustain all further LED processing steps including the subsequent removal of the original substrate by wet-chemical etching.

In order to maximize the extraction efficiency, light absorption at the bonding interface should be minimized and high reflectivities should be attained. However, to achieve low contact resistances, an annealing step is required during which the reflectivity of the metal bond may degrade. A thin dielectric layer inserted between the semiconductor and the bonding metal helps to avoid thermal degradation of the metal; current flow is enabled through defined openings in the dielectric.[37,39]

A distinct advantage of TF technology is the possibility to structure the AlGaInP surface before the bonding process. This results in a significant increase of the extraction efficiency since the geometrical shapes such as cones or spheres act as microreflectors ''buried'' at the bonding interface between the semiconductor and the carrier.

VII. CONCEPTS FOR REFLECTING STRUCTURES

There are different ways to obtain highly reflective coatings in the visible wavelength region. Metallic layers provide robust reflectors capable of reflecting visible light over a wide range of wavelengths and incident angles. Metals reflect visible light since this frequency range is well below typical plasma frequencies of the free electron gas. However, electron oscillations induced by incident light waves not only result in reflection but also in absorption caused by electron phonon scattering.

DBRs are periodic structures with a unit cell of two dielectric layers having different refractive indices n_i and thicknesses $d_i (i=1,2)$. DBRs can be regarded as one-dimensional photonic crystals with a high-reflectivity stop band (''photonic gap'') comprising the nonpropagating light states in the crystal. DBRs are usually designed to have a certain center wavelength λ_{center} at perpendicular incidence. However, the DBR reflectivity depends on the incidence angle ϕ such that the stop band shifts towards shorter wavelengths for increasing ϕ without changing its spectral width.[44] As a result, at *oblique* incidence angles λ_{center} lies in many cases no longer within the high-reflectivity region.

The reflection properties of metals and DBRs also depend on the polarization of the incident lightwave. According to Brewster's law, the reflection of light polarized parallel to the plane of incidence (TM mode) has a minimum at the incidence angle

$$\tan \phi_B = \frac{n_1}{n_2}, \tag{4}$$

where n_1 and n_2 are the refractive indices of the adjacent materials. This is particularly important for DBRs where the overall reflectivity significantly decreases at ϕ_B. DBRs with improved wide-angle reflectivity can be achieved, e.g., using aperiodically stacked layers with thickness gradients or random thickness distributions.[45,46]

Much research was devoted to DBRs with a complete photonic band gap represented by a certain frequency range where all incoming photons regardless of their momentum vector $\hbar\mathbf{k}$ are reflected. These ODRs have a wide range of interesting applications such as all-dielectric coaxial waveguides,[47] omnidirectional mirror fibers,[48] and light transport tubes.[49]

Omnidirectional reflection characteristics have been obtained using polystyrene and tellurium layers in a DBR.[50] Due to the large difference of the refractive indices, $n_{\text{polystyrene}} = 1.8$ and $n_{\text{tellurium}} = 5$, the Brewster angle ϕ_B is much larger than the critical angle ϕ_c for total reflection resulting in a nearly complete photonic band gap in the wavelength range from 10 to 15 μm.

Another intriguing approach consists of the use of birefringent polymers in DBRs with two different refractive indices parallel and vertical to the DBR layer planes.[49] By adjusting the differences between the vertical and in-plane indices the value of the Brewster angle can be controlled. Brewster angles up to 90° (grazing incidence) and even imaginary values are possible resulting in high reflectivity for TM-polarized light at virtually all incident angles.

Besides material properties such as the radiative recombination efficiency[10] one of the most important figures-of-merit for LEDs is the extraction efficiency $\eta_{\text{extraction}}$ defined as the number of photons emitted into open space relative to the number of photons generated in the active region.

The value of $\eta_{\text{extraction}}$ is limited by the fact that light emitted from the active region may be subjected to total reflection at the LED surface (see Fig. 11). The critical angle ϕ_c for total reflection is given by Snell's law

Downloaded 10 Mar 2004 to 128.113.123.154. Redistribution subject to AIP license or copyright, see http://jap.aip.org/jap/copyright.jsp

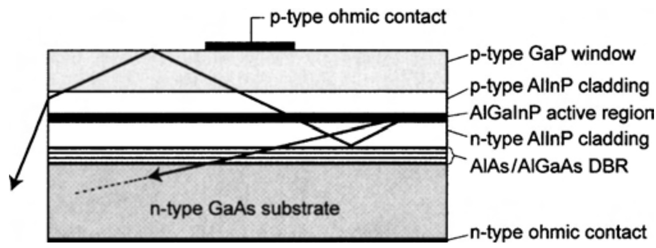

FIG. 11. Schematic of a standard AS-LED incorporating a DBR. Light rays totally reflected at the surface and the DBR are indicated in red.

$$\sin \phi_c = \frac{n_{\text{out}}}{n_s}, \tag{5}$$

where n_s and n_{out} denote the refractive indices of the semiconductor and the outside medium, respectively.

As an example, the AlGaInP material system has a value of $\phi_c \approx 17°$ with air as outside medium which in turn means that about 96% of the light emitted from the active region is reflected at the surface (we used $n_s = 3.4$ at $\lambda = 650$ nm for GaP as the semiconducting material). This value can be reduced to about 88% by embedding the LED in epoxies with high refractive indices of $n_{\text{epoxy}} \approx 1.5$.[3]

Distributed Bragg reflectors can be used as substrate coating to enhance the light extraction.[24,51] However, the active region of a LED emits light isotropically and therefore the poor DBR reflectivity at oblique incidence angles results in undesired losses particularly for waveguided modes as discussed above.

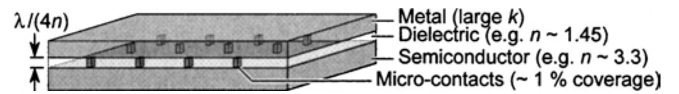

FIG. 12. Perspective view of the ODR. In the ODR-LED, the ODR serves as ohmic contact.

Unfortunately the applicability of the above-mentioned omnidirectional DBRs in LEDs is limited since they are electrically insulating. In addition, these DBR structures present a considerable thermal barrier preventing efficient heat sinking due to their large thermal resistance combined with large thickness.

VIII. OMNIDIRECTIONAL REFLECTOR (ODR) FOR LEDs

Here we describe a very promising omnidirectional reflector suitable for use in future large-area LEDs.[52] The reflector comprises the LED semiconductor material emitting at a wavelength λ_0, a low-refractive index layer (n_{li}), and a metal with a complex refractive index $N_m = n_m + ik_m$ as shown in Fig. 12.

At perpendicular incidence, the reflectance of the triple-layer ODR is given by

$$R_{\text{ODR}}(\phi=0) = \frac{\{(n_S - n_{\text{li}})(n_{\text{li}} + n_m) + (n_S + n_{\text{li}})k_m\}^2 + \{(n_S - n_{\text{li}})k_m + (n_S + n_{\text{li}})(n_{\text{li}} - n_m)\}^2}{\{(n_S + n_{\text{li}})(n_{\text{li}} + n_m) + (n_S - n_{\text{li}})k_m\}^2 + \{(n_S + n_{\text{li}})k_m + (n_S - n_{\text{li}})(n_{\text{li}} - n_m)\}^2}. \tag{6}$$

Equation (6) is calculated for a phase thickness of the low-index layer corresponding to $\lambda_0/(4n_{\text{li}})$ ("quarter wave layer"). For an AlGaInP/SiO_2/Ag structure emitting at $\lambda = 630$ nm, Eq. (6) yields a normal-incidence reflectance $R_{\text{ODR}}(\theta=0) > 98\%$. This value exceeds the corresponding value for a structure without low-index layer by about 3%, thereby reducing optical losses by a substantial amount.

The omnidirectional reflection characteristics can be attributed to an imaginary interfacial Brewster angle ϕ_B similar to the birefringent DBRs. For an ODR consisting of just a semiconductor and a metal layer, the Brewster angle is given by

$$\tan \phi_B = \frac{n_m}{n_s} + i\frac{k_m}{n_s}. \tag{7}$$

An analogous relationship is valid if an intermediate dielectric layer is used. The magnitude of the imaginary part in Eq. (7) determines how strongly the reflectivity decrease of TM-polarized light at ϕ_B is suppressed. As can be inferred from Eq. (7), a criterion to maintain high reflectivity is to maximize k_m/n_s and minimize n_m/n_s. In an AlGaInP-based LED ($n_s = 3.3$) emitting at $\lambda = 630$ nm silver ($n_m = 0.08, k_m = 4$) is a particularly good choice as compared to other metals such as gold ($n_m = 0.18, k_m = 2.4$) or nickel ($n_m = 2.1, k_m = 3.6$).

Figure 13 compares different triple-layer ODRs to a transparent DBR widely used in AlGaInP-based LEDs. While the ODRs maintain high reflectivity at virtually all

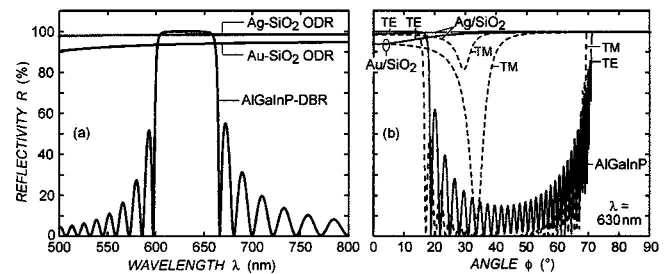

FIG. 13. Calculated reflectivity for two ODRs and a DBR with a center wavelength at 630 nm. GaP was chosen as the external medium. The transparent AlGaInP DBR consists of 35 $[(Al_{0.3}Ga_{0.7})_{0.5}In_{0.5}P/Al_{0.5}In_{0.5}P]$ pairs. The ODRs have a 500 nm thick metal layer covered by a quarter wave thick SiO_2 layer on a GaAs substrate: (a) reflectivity vs wavelength for normal incidence and (b) angular dependence of the reflectivity at 630 nm. The solid and dashed lines correspond to transverse electric and transverse magnetic polarized waves, respectively.

Downloaded 10 Mar 2004 to 128.113.123.154. Redistribution subject to AIP license or copyright, see http://jap.aip.org/jap/copyright.jsp

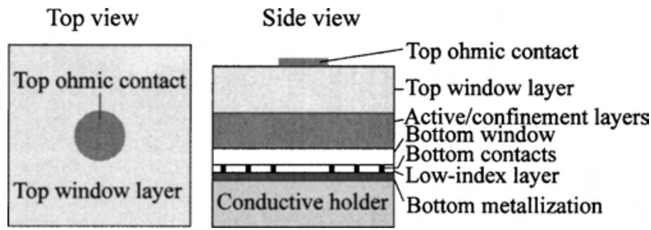

FIG. 14. Schematic of the ODR-LED. An array of microcontacts perforating the ODR serves as *p*-type ohmic contact to the epitaxial AlGaInP layers.

angles of incidence, the DBR reflectivity sharply drops above 17°. The curves shown in Fig. 13 were calculated numerically using the optical transfer-matrix method.[44] It can be inferred from Fig. 13 that triple-layer ODRs perform significantly better at oblique angles of incidence than transparent DBRs. This illustrates the substantial gain brought about by the use of ODRs in LEDs.

The ODR described here can be used with low-cost Si substrates using conductive epoxy or by means of a metal-to-metal bonding process. These bonding processes have much less stringent requirements than direct semiconductor-to-semiconductor wafer bonding processes as used for TS-LEDs. The schematic structure of the ODR-LED is shown in Fig. 14. It consists of a top current-spreading (or window) layer, the active and confinement layers, a bottom window layer, the ODR, and a submount such as a Si or metal wafer. The active layers include the lower and upper confinement layers and the bulk or MQW active region. The wafer is grown in the standard "*p*-side up" mode that is employed in nearly all AlGaInP LEDs at the present time.

As shown in Fig. 14, the low-index layer is perforated by many small ohmic contacts that cover only a small fraction of the entire backside area of the LED die. The array of microcontacts allows the electrical current to pass through the dielectric layer. Assuming that the ohmic contacts have an area of 1% of the die, and that the alloyed ohmic contact metal is 50% reflective, the reflectivity of the ODR is reduced by only 0.5%.

Because the LED active region emits light isotropically, the total substrate reflectivity averaged over the solid angle would be a suitable figure-of-merit. The average reflectivity is given by

$$\bar{R}(\lambda)=\frac{1}{2\pi}\int_0^{\pi/2}R(\lambda,\phi)2\pi\sin\phi d\phi, \tag{8}$$

where λ denotes the emission wavelength and ϕ the angle of incidence. Values of $\bar{R}$ for different reflectors are calculated by numerical integration of the reflectivity curves shown in Fig. 13 and are listed in Table I. The averaged reflectivity of triple-layer ODRs exceeds the value of $\bar{R}$ for the transparent DBR by about a factor of 2. A reflectivity gain by a factor of 2.1 is obtained for the Ag–SiO_2 ODR.

Note that the reflectivity increase is significant and substantial. For a loss less medium, the power of a waveguided mode, P, attenuated by multiple reflection events (with reflectivity R) depends on the number of reflection events, N, according to

TABLE I. Values of the angle-integrated reflectivity $\bar{R}$ at 630 nm calculated from Eq. (8) using the theory curves such as shown in Fig. 13(b). The metal–ODRs consist of a 500 nm thick metal layer covered by a quarter wave SiO_2 layer on a GaAs substrate. The transparent AlGaInP–DBR consists of 35 $[(Al_{0.3}Ga_{0.7})_{0.5}In_{0.5}P/Al_{0.5}In_{0.5}P]$ quarter wave pairs. The values of n_m, n_1, n_h correspond to the refractive indices of the metals and the low-/high-index layers in the DBRs, k_m denotes the metal-extinction coefficient. GaP was chosen as outside medium for all reflectors ($n_S=3.3$ for GaP at $\lambda=630$ nm).

Reflector type	Refractive index ($\lambda=630$ nm)	Extinction coefficient ($\lambda=630$ nm)	$\bar{R}$ ($\lambda=630$ nm)
Ag–SiO_2 ODR	$n_m=0.08$	$k_m=4$	0.994
Au–SiO_2 ODR	$n_m=0.18$	$k_m=2.7$	0.962
Ni–SiO_2 ODR	$n_m=2.1$	$k_m=3.6$	0.932
AlGaInP–DBR	$n_1=2.9$, $n_h=3.35$	Transparent	0.473

$$P=P_0R^N, \tag{9}$$

where P_0 is the initial power of the mode. This equation illustrates that R is of great importance due to the power-law dependence. High values of R are essential to minimize waveguide losses. This consideration shows the tremendous advantage offered by ODRs.

The wide-angle reflectivity of the ODR allows wave guiding of light rays with much smaller attenuation than a DBR. As a result, light extraction at the edges of the LED chip is strongly increased. In addition, the top surface of the ODR-LED may be rougher than the surface of the DBR-LED due to the etching used for the substrate removal. Assuming random surface roughness, photons are either scattered isotropically or totally reflected with a random distribution of reflection angles. As a result, photon outcoupling from waveguided modes into vertical radiation modes is drastically enhanced during round trips between the surface and ODR.

IX. CHARACTERISTICS OF ODR-LEDs

The ODR-LED technology does not exhibit the optical losses of AS-LEDs and DBR-LEDs due to the employment of a high-reflectivity omnidirectional reflector. Therefore a significant performance advantage for ODR-LED compared with AS-LEDs and DBR-LEDs can be obtained.

Figure 15 compares the current injection patterns for AS-, TS-, and ODR-LEDs. Inspection of the figure reveals that both AS and TS technologies have maximum current density under the top contact. Since the top contact is opaque and has low reflectivity, light generated below the contact is

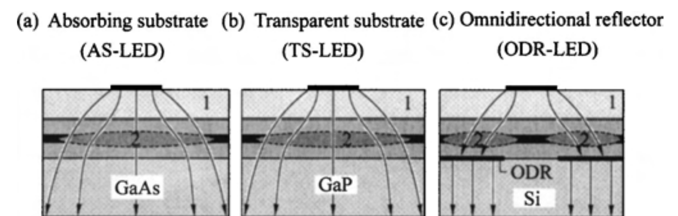

FIG. 15. Current distribution and size of light-emitting region in AS-, TS-, and ODR-LEDs. "1" denotes the current spreading layer and "2" the region of light emission.

Downloaded 10 Mar 2004 to 128.113.123.154. Redistribution subject to AIP license or copyright, see http://jap.aip.org/jap/copyright.jsp

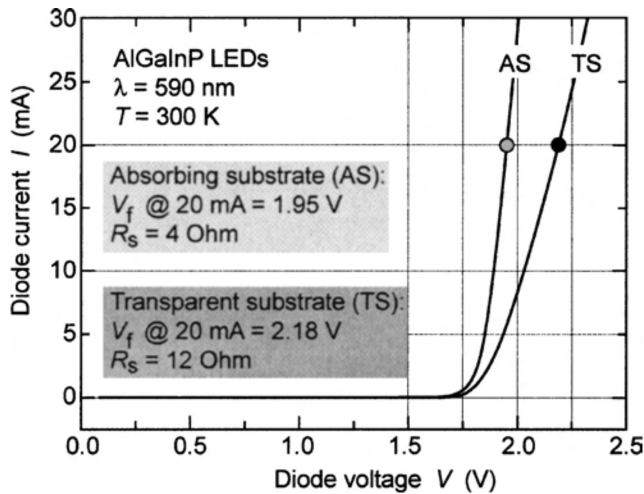

FIG. 16. Current vs voltage characteristic of an AS-LED and a TS-LED.

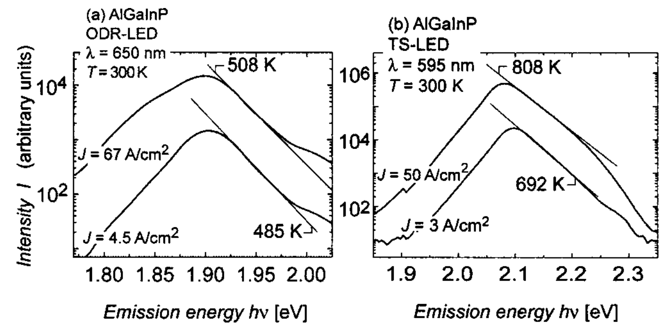

FIG. 17. Electroluminescence spectra of an ODR-LED ($\lambda = 650$ nm) and a TS-LED ($\lambda = 595$ nm) measured at different values of the drive current density J. The slope of the high-energy side of the electroluminescence peak is proportional to the active region temperature. The straight lines are fits to the experimental data.

blocked. The ODR-LED avoids these optical losses due to a patterned backside contact that results in a current injection pattern minimizing the current flow under the top contact. Patterning of the backside contact would *not be effective* to AS- and TS-LEDs because the highly conductive substrates (GaAs and GaP) effectively spread the current along lateral directions.

The comparison of the AS and TS current–voltage ($I-V$) characteristics shown in Fig. 16 illustrates that TS-LEDs have a slightly higher forward voltage. The heterojunction band discontinuity occurring at the semiconductor-to-semiconductor wafer-bonded interface, low doping of the GaP substrate (to avoid free-carrier absorption), and interfacial oxides are possible reasons for the forward-voltage penalty in TS-LEDs. As a result of the higher forward voltage, the electrical input power increases and the luminous performance is reduced. For ODR-LEDs no such forward-voltage penalty is expected.

The Si or metal submounts employed in the ODR-LED have a high thermal conductivity. This can be seen in Table II, which compares the thermal conductivity of GaAs, GaP, Si, Cu, and sapphire. Even though metal substrates have much higher thermal conductivity than any semiconductor, the higher thermal conductivity of Si submounts will already allow for lower active region temperatures and thus higher drive currents as compared to the GaAs or GaP. In addition, the greater mechanical stability of Si wafers will enable thinner submounts as compared to TS or AS devices, thus allowing for improved heat sinking. The low-index dielectric layer used for the ODR has a negligible influence on the thermal conductance due to its small thickness $[\lambda/(4n) \approx 110 \text{ nm}]$.

Electroluminescence spectra of an Ag-based ODR-LED attached to a conductive Si substrate with silver epoxy and a TS-LED emitting at 595 nm are shown in Fig. 17. The spectra were measured at two different drive current values in order to study the effect of active region heating on both devices. Devices were isolated by wet-chemical etching (ODR-LED) or cleaved from the wafer (TS-LED) with junctions areas $A_j \approx 0.05 \text{ mm}^2$ (TS-LED) and $A_j \approx 0.09 \text{ mm}^2$ (ODR-LED). In the heating experiment the drive current was chosen such that the current densities in the two devices were comparable assuming uniform current distribution across the junction area. The slope of the high-energy side of the electroluminescence band is proportional to

$$\text{intensity} \propto \exp[-(h\nu/kT)]. \quad (10)$$

As the straight-line fits in Fig. 17 show, the slope indeed becomes smaller with increasing drive current indicating a temperature rise of the active region. This change is more pronounced for the TS-LED indicating stronger heating of the device.

The lower device heating of the ODR-LED can be attributed to the higher thermal conductivity of the Si substrate. However, it is important to note that the heating of AlGaInP LEDs increases towards shorter emission wavelengths. This is caused by the decreasing confinement barrier height allowing more carriers to leave the active region and the resulting lower internal radiative efficiency. The thermal conductivity of Si is about 300% larger than in GaAs and about 50% higher than in GaP. As a result, the active region is less heated in ODR-LEDs as compared to AS- and TS-LEDs. This is an important feature for high-power LEDs since it allows operating ODR devices at higher injection currents and higher optical power levels. In addition, Si substrates are available at much lower cost than compound semiconductor substrates.

Micrographs of an Ag-based ODR-LED under external illumination and under operation are shown in Figs. 18(a) and 18(b), respectively. The emission occurs in the red part of the spectrum with a peak wavelength of 650 nm. The pattern of small-area ohmic contacts beneath the large area top contacts can be clearly seen. In Fig. 18(a), the small-area contacts appear dark because their reflectivity is lower than

TABLE II. Thermal conductivity of GaAs, GaP, Si, Cu, and sapphire at room temperature.

Material	GaAs	GaP	Si	Cu	Sapphire
Thermal conductivity W/(cm K)	0.5	1.1	1.5	3.85	0.35

Downloaded 10 Mar 2004 to 128.113.123.154. Redistribution subject to AIP license or copyright, see http://jap.aip.org/jap/copyright.jsp

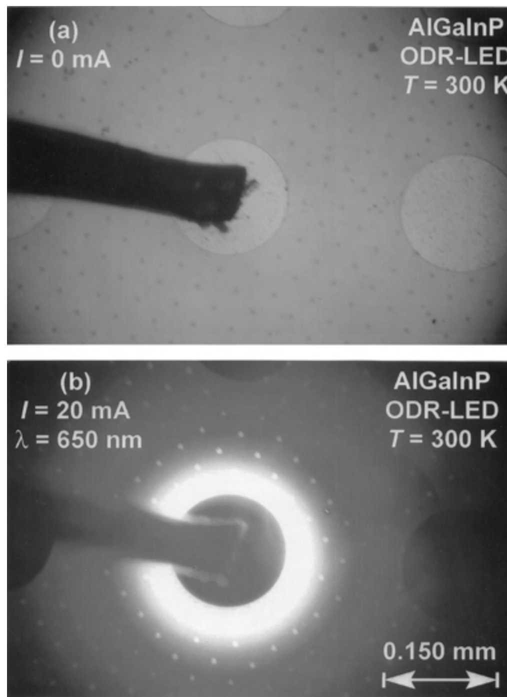

FIG. 18. (a) Micrograph of an AlGaInP ODR-LED with Ag reflector bonded with silver epoxy to conductive Si under external illumination. (b) Micrograph of the same ODR-LED with current injection ($I=20$ mA).

the reflectivity of the surrounding ODR. In Fig. 18(b), however, the small contacts are brighter indicating light emission in their vicinity.

Optical output power P versus injection current I for an Ag ODR-LED bonded with silver epoxy to conductive Si, an AS-LED with a DBR, and a TS-LED are shown in Fig. 19. The peak wavelengths of the three devices are 650 nm (ODR-LED), 630 nm (DBR-LED), and 595 nm (TS-LED) with junction areas $A_j \approx 0.09$, 0.25, and 0.05 mm^2, respectively. In order to measure the total optical output power the samples were placed on a reflecting holder inside an integrating sphere.

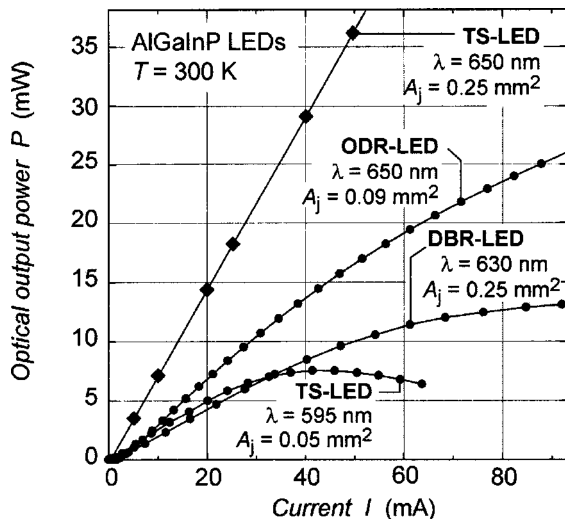

FIG. 19. Dependence of the total optical output power on the drive current for AlGaInP LEDs with different emission wavelengths λ and junction areas A_j. The samples were placed on a reflective sample holder inside an integrating sphere for the measurements. The data for the red TS-LED are taken from Ref. 33.

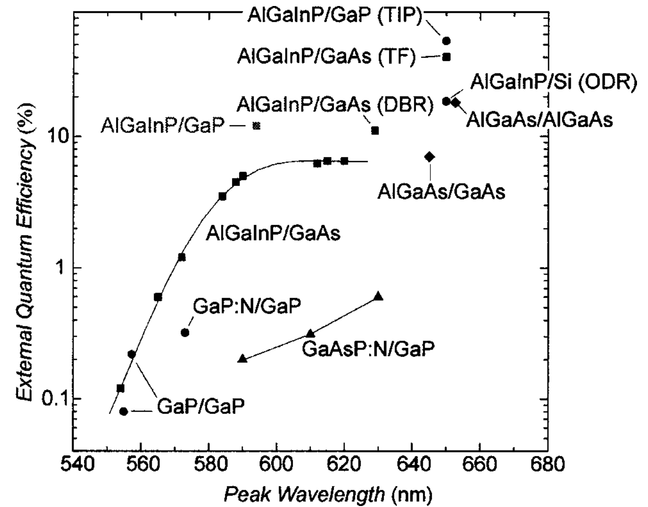

FIG. 20. External quantum efficiency for different LEDs. Data points are labeled with epitaxial material and the substrate (epi/substrate). (Data taken from Refs. 26, 33, 41, and this work.)

The largest light output is attained by the ODR-LED. Maximum values of the external quantum efficiencies η_{ext} are about 18% for the ODR device ($I_f=27$ mA), 11% for the DBR-LED ($I_f=27$ mA), and 12% for the TS-LED ($I_f=11$ mA). TS-LEDs operating at 632 nm have an excellent external efficiency of 32%,[31] about a factor of 2 higher than the ODR-LED shown in Fig. 19. The external quantum efficiency of the ODR device is expected to further increase with a thicker top window layer. The window layer thickness of the ODR device shown in Fig. 19 is 2.0 μm and it is reasonable to expect an improvement by a factor of 2 for optimized ODR devices with a thick window layer.

In the linear region of the light-output-power versus current curves of Fig. 19 the DBR-LED emits clearly the smallest optical power even though it has a larger internal efficiency than the TS-LED corresponding to its longer emission wavelength. This is direct evidence of the high extraction efficiency of transparent substrate devices. (An AS-LED without the DBR has even lower output power than the DBR-LED and is therefore not shown in the figure).

Inspection of Fig. 19 shows that the saturation of the optical output power is smallest for the ODR-LED. The saturation may be caused by carrier overflow over the confinement barriers. Taking into account the differences in the junction areas A_j of the ODR- and AS-LED this can be attributed to the better thermal conductivity of the Si holder as compared to GaAs. The pronounced saturation effect in the TS-LED is likely caused by the smaller confinement barrier height allowing more carriers to flow over the barrier.

Figure 20 compares the external quantum efficiencies η_e of the TS, AS, and ODR-LED to values obtained for other material systems in particular to AlGaInP-based LEDs with a thick window layer. Even in the present state the external quantum efficiency of the ODR-LED is about 1.6 times larger than η_{ext} of the DBR-LED.

Downloaded 10 Mar 2004 to 128.113.123.154. Redistribution subject to AIP license or copyright, see http://jap.aip.org/jap/copyright.jsp

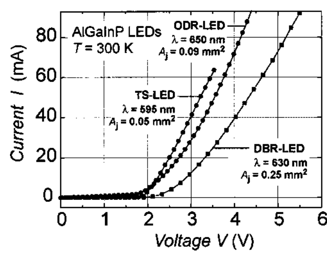

FIG. 21. Current vs voltage characteristics for ODR-, DBR-, and TS-LEDs emitting at 650, 630, and 595 nm, respectively. The junction areas A_j are about 0.09 mm^2 for ODR- and AS-LEDs and about 0.05 mm^2 for the TS-LED.

The $I-V$ characteristic of an AlGaInP ODR-LED is shown in Fig. 21. At a current of 20 mA, the forward voltage is about 2.7 V. For comparison, the $I-V$ characteristics of an AlGaInP DBR-LED and TS-LED are also shown in the figure. It should be noted that the $I-V$s of DBR- and ODR-LEDs do not result from optimized processes or optimized top layers for low-ohmic contact resistances as in the case of the TS device.

X. WAFER BONDING FOR AlGaInP ODR-LEDs

Two fabrication routes for AlGaInP-based ODR LEDs (n-type up or p-type up) are shown schematically in Figs. 22 and 23. Both processes start out with "p-side up" epiwafers, which are the standard for epitaxial growth, and include front- and backside processing of the ODR-LED, removal of the original substrate, and bonding to a conductive carrier. The conductive carrier should ensure good heat sinking and should be thermal-expansion matched with respect to the epilayer.

The p-type up process involves more steps (due to the use of a temporary holder), but has the potential for lower contact resistances at the LED backside contact since the small-area contact pattern is applied to n-type material. The n-type up process does not require a temporary holder but the backside ohmic contacts are to p-type material, which likely results in higher contact resistances.

Chemo-mechanical polishing can be employed to thin the GaAs wafer down to a thickness of about 50–100 μm. The remaining layer can then be removed by selective wet chemical etching. The wet-chemical etching step, however, requires one or more etch stop layers covering the bottom

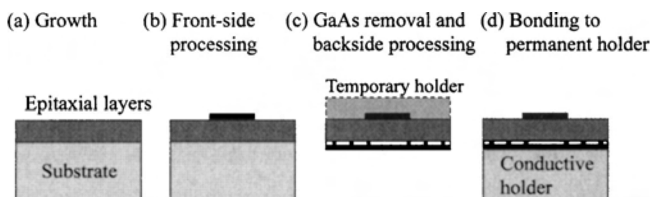

FIG. 22. Schematic process for a "p-type up" ODR light-emitting diode. After epitaxial growth (a), large area p-type contacts are applied to the front side of the ODR-LED (b). The wafer is then attached to a temporary top holder by means of wax or a similar substance; after removal of the original substrate, the n-type microcontact pattern with dielectric and metal reflector is defined on the backside of the ODR LED (c). Finally, the wafer is bonded to a conductive permanent holder (d).

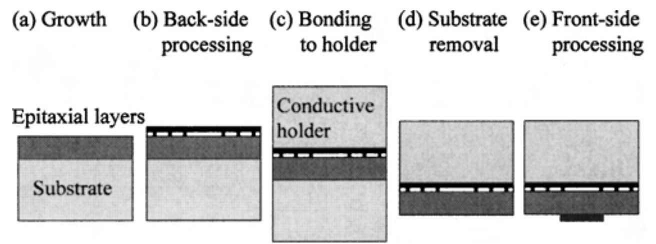

FIG. 23. Schematic process for an n-type up ODR light-emitting diode. After epitaxial growth (a), the p-type microcontact pattern with dielectric and metal layers is defined on the backside of the ODR LED (b). The wafer is then bonded to the conductive carrier (c). Finally, the original substrate is removed and large area n-type contacts are applied to the front side of the ODR-LED (d), (e).

window layer of the LED to prevent etch damage. With optimized thickness, composition, and sequence of several etch stop layers the damage to the lower window layer can be minimized.

The epitaxial ODR LED layer needs to be bonded to a permanent holder. Several materials are suited as holders: Si and metal substrates have high thermal conductivity when compared to GaAs or GaP and therefore provide for efficient heat sinking. However, suitable holder materials have to ensure thermal expansion matching, which is required to avoid stress damage to the LED during processing steps at elevated temperatures.

The bonding process has to result in a uniform large-area bond between the substrate and the LED, which is able to sustain temperature cycling required during further LED processing such as annealing of electrical contacts. Furthermore, the wafer bonding process should be compatible with a 4 in. process.

The bond may be accomplished by forming a binary intermetallic compound located between the conductive holder and the LED epilayer. For this purpose, the bonding surfaces may be covered either directly with the alloy[53] or with the two separate components in a layer sequence with individual thicknesses ensuring the correct alloy composition.[54,55] Subsequently the two surfaces are stacked face-to-face and annealed. The bonding is mediated by solid phase reactions such as solid-phase epitaxial regrowth at the alloy/epilayer and the alloy/holder interfaces. Preferably, it also involves liquid-phase reactions that help to reduce surface roughness.[54,55] The bonding material should adhere to the LED epilayer as well as to the holder and should have low electrical resistance. The bonding process should take place at sufficiently low temperatures in order to avoid dopant redistribution in the heterostructure. Note that the requirements for the bonding process discussed above are less critical than for the semiconductor-to-semiconductor bonding processes used in TS technology.

As an example, the AuGe intermetallic compound is capable of forming low-resistivity contacts to n-type GaAs and can therefore be employed to bond the ODR-LED epilayer to a GaAs holder. AuGe forms a eutectic phase during the bonding process at temperatures close to the melting point $T_m = 360\,^\circ$C of the eutectic. Other systems such as PdIn with

Downloaded 10 Mar 2004 to 128.113.123.154. Redistribution subject to AIP license or copyright, see http://jap.aip.org/jap/copyright.jsp

a transient liquid phase have been used for bonding of GaN epilayers to Si.[54,55]

An alternate possibility to permanently bond the epilayer to a holder is the use of silver-loaded epoxy. The epoxy offers excellent electrical conductivity, adhesion, and bond strength. It can be easily and uniformly dispensed on the sample and is extremely reliable. However, during subsequent contact annealing the degradation temperature of the epoxy polymer $T_D \approx 400\,^{\circ}\mathrm{C}$ must not be exceeded. In addition, the thermal expansion is different from GaP and therefore thermal expansion matching is difficult.

XI. CONCLUSIONS

In this review AlGaInP structures suited for LEDs operating in the red, orange, yellow, and yellow–green wavelength range were discussed. These devices will play a key role in solid-state lighting applications. One of the most important requirements for use of LEDs in solid-state lighting is the attainment of very large light extraction efficiencies. For this reason this review placed particular emphasis on device structures allowing for high-brightness light emission. These structures overcome the inherent light loss due to the absorbing GaAs substrate in standard AlGaInP LEDs by either replacing GaAs with a transparent GaP carrier or by covering it with reflectors. TS LEDs have attained record external quantum efficiencies of 55% exceeding the efficiency of AS LEDs by a factor of 10. However, their cost of manufacturing is high due to the employment of GaP substrates, a critical wafer-bonding process, and a thick GaP window layer.

LEDs employing a DBR inserted between the GaAs substrate and the lower window layer are widely used types of reflector-enhanced devices. These DBR-LEDs offer higher light extraction efficiencies than AS-LEDs, yet they are plagued by the fact that the excellent reflective properties of DBRs are limited to vertically incident light. These drawbacks are avoided by TS-LEDs and TF-LEDs, which utilize metal-to-metal wafer fusion techniques and attained large quantum efficiencies as high as 40%.

The recently developed high-reflectivity, electrically conductive ODRs are able to considerably outperform conventional DBR's. The ODR can be integrated as a *p*-type contact into an AlGaInP-based LED emitting at 650 nm. After removal of the original GaAs substrate using mechanical polishing and wet-chemical etching, the ODR LED is mounted on a conductive Si with silver-loaded epoxy. The ODR-LED has been compared to an AlGaInP-based LED with a conductive DBR covering the GaAs substrate (DBR-LED). From measurements of the optical output power versus forward current external quantum efficiencies of about 18% and 11% have been obtained for ODR- and AS-LED, respectively. In addition, the Si substrate has superior heat conductivity compared to GaAs and GaP substrates and allows operating the device at potentially high current density and light output levels. Different generic methods can be utilized to increase light extraction of all the device structures mentioned above. As examples, techniques to pattern LED surfaces with random or regular structures in particular with photonic crystals have been presented. Shaping of the entire chip has proven extremely beneficial in the case of TS-LEDs and enabled the record efficiencies obtained by these devices.

AlGaInP LEDs are extremely promising devices for high-power solid-state lighting applications. In particular, high-brightness red LEDs using ODRs can be employed in high-efficiency trichromatic and tetrachromatic white light sources. This will enable production of white light with high color rendering indexes in future solid-state lighting applications.

[1] E. F. Schubert, *Light Emitting Diodes* (Cambridge University Press, Cambridge, U.K., 2003).
[2] F. M. Steranka, in *High Brightness Light Emitting Diodes*, edited by G. B. Stringfellow and M. G. Craford, Semiconductors and Semimetals Vol. 48 (Academic, San Diego, 1997), pp. 65–95 and references therein.
[3] F. A. Kish and R. M. Fletcher, in *High Brightness Light-Emitting Diodes*, edited by G. B. Stringfellow and M. G. Craford, Semiconductor and Semimetals, Vol. 48 (Academic, San Diego, 1997), pp. 149–220 and references therein.
[4] C. H. Chen, S. A. Stockman, M. J. Peanasky, and C. P. Kuo, in *High Brightness Light Emitting Diodes*, edited by G. B. Stringfellow and M. G. Craford, Semiconductors and Semimetals, Vol. 48 (Academic, San Diego, 1997), pp. 97–144 and references therein.
[5] Y.-L. Li, Th. Gessmann, and E. F. Schubert, Proceedings SPIE Annual Meeting, San Diego, August 4–8, 2003.
[6] K. Kobayashi, S. Kawata, A. Gomyo, I. Hino, and T. Suzuki, Electron. Lett. **21**, 931 (1985).
[7] Y. Ohba, M. Ishikawa, H. Sugawara, T. Yamamoto, and T. Nakanisi, J. Cryst. Growth **77**, 374 (1986).
[8] M. Ikeda, K. Nakano, Y. Mori, K. Kaneko, and N. Watanabe, J. Cryst. Growth **77**, 380 (1986).
[9] K. Itaya, M. Ishikawa, and Y. Uematsu, Electron. Lett. **26**, 839 (1990).
[10] See, for example, *High Brightness Light-Emitting Diodes*, edited by G. B. Stringfellow and M. G. Craford, Semiconductors and Semimetals, Vol. 48 (Academic, San Diego, 1997).
[11] See, for example, *Electroluminescence I*, edited by G. Mueller, Semiconductors and Semimetals, Vol. 64 (Academic, San Diego, 2000).
[12] M. R. Krames, H. Amano, J. J. Brown, and P. L. Heremans, IEEE J. Sel. Top. Quantum Electron. **8**, 185 (2002).
[13] C. P. Kuo, R. M. Fletcher, T. D. Osentowski, M. C. Lardizabel, M. G. Craford, and V. M. Robbins, Appl. Phys. Lett. **57**, 2937 (1990).
[14] R. M. Fletcher, C. P. Kuo, T. D. Osentowski, and V. M. Robbins, US Patent No. 5,008,718 (1991).
[15] H. Sugawara, M. Ishikawa, and G. Hatakoshi, Appl. Phys. Lett. **58**, 1010 (1991).
[16] H. Sugawara, M. Ishikawa, Y. Kokubun, Y. Nishikawa, and S. Naritsuka, U.S. Patent No. 5,048,035 (1991).
[17] G. H. B. Thompson, *Physics of Semiconductor Laser Devices* (Wiley, New York, 1980).
[18] R. M. Fletcher, C. P. Kuo, T. D. Osentowski, K. H. Huang, and M. G. Craford, J. Electron. Mater. **20**, 1125 (1991).
[19] H. Sugawara, M. Ishakawa, Y. Kokubun, Y. Nishikawa, S. Naritsuka, K. Itaya, G. Hatakoshi, and M. Suzuki, United States Patent No. 5,153,889 (1992).
[20] H. Sugawara, K. Itaya, H. Nozaki, and G. Hatakoshi, Appl. Phys. Lett. **61**, 1775 (1992).
[21] K.-H. Huang and T.-P. Chen, U.S. Patent No. 5,661,742 (1997).
[22] S. J. Chang and C. S. Chang, IEEE Photonics Technol. Lett. **10**, 772 (1998).
[23] S. J. Chang and C. S. Chang, Jpn. J. Appl. Phys., Part 2 **37**, L653 (1998).
[24] T. Kato, H. Susawa, M. Hirotani, T. Saka, Y. Ohashi, E. Shichi, and S. Shibata, J. Cryst. Growth **107**, 832 (1991).
[25] S. J. Chang, C. S. Chang, Y. K. Su, P. T. Chang, Y. R. Wu, K. H. Huang, and T. P. Chen, IEE Proc.: Optoelectron. **144**, 1 (1997).
[26] K.-H. Huang, J. G. Yu, C. P. Kuo, R. M. Fletcher, T. D. Osentowski, L. J. Stinson, M. G. Craford, and A. S. H. Liao, Appl. Phys. Lett. **61**, 1045 (1992).
[27] F. A. Kish *et al.*, Appl. Phys. Lett. **64**, 2839 (1994).
[28] L. W. Cook, M. D. Camras, S. L. Rudaz, and F. M. Steranka, in *Proceed-*

Downloaded 10 Mar 2004 to 128.113.123.154. Redistribution subject to AIP license or copyright, see http://jap.aip.org/jap/copyright.jsp

ings of the 14th International Symposium on GaAs and related Compounds 1987 (Institute of Physics, Bristol, 1988), pp. 777–780.
[29] F. A. Kish, D. A. Vanderwater, M. J. Peanasky, M. J. Ludowise, S. G. Hummel, and S. J. Rosner, Appl. Phys. Lett. **67**, 2060 (1995).
[30] G. E. Hoefler, D. Vanderwater, D. C. DeFevere, F. A. Kish, M. Camras, F. Steranka, and I.-H. Tan, Appl. Phys. Lett. **69**, 803 (1996).
[31] N. F. Gardner *et al.*, Appl. Phys. Lett. **74**, 2230 (1999).
[32] M. Boroditsky and E. Yablonovitch, Proc. SPIE **3002**, 119 (1997).
[33] M. R. Krames *et al.*, Appl. Phys. Lett. **75**, 2365 (1999).
[34] H. W. Deckman and J. H. Dunsmuir, Appl. Phys. Lett. **41**, 377 (1982).
[35] R. Windisch *et al.*, Appl. Phys. Lett. **79**, 2315 (2001).
[36] N. Linder, S. Kugler, P. Strauss, R. Wirth, H. Zull, and K. P. Streubel, Compound Semicond. **7**, 59 (2001).
[37] K. Streubel, N. Linder, R. Wirth, and A. Jaeger, IEEE J. Sel. Top. Quantum Electron. **8**, 321 (2002).
[38] A. Erchak, D. J. Ripin, S. Fan, P. Rakich, J. D. Joannopoulos, E. P. Ippen, G. S. Petrich, and L. A. Kolodziejski, Appl. Phys. Lett. **78**, 563 (2002).
[39] S. Illek, U. Jacob, A. Ploessl, P. Strauss, K. Streubel, W. Wegleiter, and R. Wirth, Compound Semicond. **8**, 39 (2002).
[40] C. Rooman, S. De Jonge, C. Karnutsch, K. P. Streubel, M. Kuijk, B. Dutta, G. Borghs, and P. L. Heremans, Proc. SPIE **4996**, 40 (2003).
[41] R. Wirth *et al.*, Proc. SPIE **4996**, 1 (2003).
[42] R. H. Horng, D. S. Wuu, S. C. Wei, M. F. Huang, K. H. Chang, P. H. Liu, and K. C. Lin, Appl. Phys. Lett. **75**, 154 (1999).
[43] R. H. Horng, D. S. Wuu, S. C. Wei, C. W. Tseng, M. F. Huang, K. H. Chang, P. H. Liu, and K. C. Lin, Appl. Phys. Lett. **75**, 3054 (1999).
[44] H. A. Macleod, *Thin-Film Optical Filters* (McGraw-Hill, New York, 1986), pp. 35–45.
[45] K. V. Popov, J. A. Dobrowolski, A. V. Tikhonravov, and B. T. Sullivan, Appl. Opt. **36**, 2139 (1997).
[46] J. Xu, H. Fang, and Zh. Lin, J. Phys. D **34**, 445 (2001).
[47] M. Ibanescu, Y. Fink, S. Fan, E. L. Thomas, and J. D. Joannopoulos, Science **289**, 415 (2000).
[48] S. D. Hart, G. R. Maskaly, B. Temelkuran, P. H. Prideaux, J. D. Joannopoulos, and Y. Fink, Science **296**, 510 (2002).
[49] M. F. Weber, C. A. Stover, L. R. Gilbert, T. J. Nevitt, and A. J. Ouderkirk, Science **287**, 2451 (2000).
[50] Y. Fink, J. N. Winn, S. Fan, Ch. Chen, J. Michel, J. D. Joannopoulos, and E. L. Thomas, Science **282**, 1679 (1998).
[51] S. W. Chiou, C. P. Lee, C. K. Huang, and C. W. Chen, J. Appl. Phys. **87**, 2052 (2000).
[52] Th. Gessmann, E. F. Schubert, J. W. Graff, and K. P. Streubel, Proc. SPIE **4996**, 26 (2003).
[53] Z. Ma, G. L. Zhou, H. Morkoc, and L. H. Allen, Appl. Phys. Lett. **64**, 772 (1994).
[54] W. S. Wong, A. B. Wengrow, Y. Cho, A. Salleo, N. J. Quitoriano, N. W. Cheung, and T. Sands, J. Electron. Mater. **28**, 1409 (1999).
[55] W. S. Wong, T. Sands, N. W. Cheung, M. Kneissl, D. B. Bour, P. Mei, L. T. Romano, and N. M. Johnson, Appl. Phys. Lett. **77**, 2822 (2000).

Downloaded 10 Mar 2004 to 128.113.123.154. Redistribution subject to AIP license or copyright, see http://jap.aip.org/jap/copyright.jsp